

(slope) and comparable absolute values for $30\text{ K} \leq T \leq 290\text{ K}$ and $0.5\text{ T} \leq H \leq 55\text{ T}$ (Fig. 3, inset). The quantum oscillations at low T are more pronounced at higher carrier density, and suggest that reducing n could extend the temperature range over which the monotonic power law scaling holds.

The $5/3$ scaling power ($\Delta\rho_{xx} \propto \rho_{xy}^{1.65 \pm 0.1}$) reflects more than the nonlinear H -dependence of the Hall resistivity (Fig. 2). Scaling works in the low-field regime where $\rho_{xy} \propto H$ and in the high-field regime where $\rho_{xy}(H)$ departs from linearity; hand-in-hand variations of $\rho_{xx}(H, T)$ and $\rho_{xy}(H, T)$ naturally conspire to produce power-law scaling over the full range of field and temperature. Collapse onto one curve (Fig. 3), however, requires the sample-specific factor $b(T)$, whose general form is illustrated in Fig. 4. We index $b(T)$ to $\rho_{xx}(H=0, T)$, noting the distinction between the constant carrier density regime below the resistance peak and the activated regime for $T > 80\text{ K}$ (ref. 1). The fact that $b(T)$ becomes markedly less T -dependent below $T \approx 80\text{ K}$ argues for a decomposition of $b(T)$ above and below T_p . At low T , ρ_{xx} increases with increasing T owing to phonon scattering, $b(T)$ is a nearly temperature-independent constant, and Kohler's rule serves as a reasonable construct for seeking universality. Complications ensue in the intrinsic semiconducting regime above T_p . We have nominally accounted for the variation of n with T and H by plotting $\Delta\rho_{xx}/\rho_0$ versus ρ_{xy}/ρ_0 rather than $H/n\rho_0$. Nonetheless, $b(T)$ rises steadily as $\rho_{xx}(T)$ falls, pointing to elements beyond semiclassical transport.

A quantum transport mechanism is certainly suggested by the pronounced oscillations in $\rho_{xx}(H)$ and $\rho_{xy}(H)$ that emerge at low T . They begin for $\rho_{xx} \approx 0.8\text{ m}\Omega\text{ cm}$, which corresponds to a sheet resistance (per unit cell layer) of $14\text{ k}\Omega$, close to the fundamental unit of resistance given by h/e^2 (where h is Planck's constant and e is the electronic charge). The oscillatory minima do not scale precisely as $1/H$, indicating a field-induced change in the electronic density of states beyond simple Landau level formation. Quantum fluctuations combined with disorder, caused for example by excess silver embedded in less-conducting material, can introduce length scales that are not set by the cyclotron radius, and can lead to a linear field dependence of the resistivity over decades in H (refs 5 and 6). (Classical approaches to inhomogeneous media¹⁵ also can account for the unusual linear magnetoresistance in non-stoichiometric Ag_2Se and Ag_2Te , but are, at present, incompatible with experiments at small $\omega_c\tau$; refs 1, 4.)

The technological promise of the silver chalcogenides lies precisely in the smooth and continued development of the magnetotransport characteristics over huge changes in applied field. Perhaps most telling, however, is the robust scaling relation that unfolds while relative energy scales change by orders of magnitude. The universal behaviour of Fig. 3 holds when the magnetic energy $g\mu_B H$ is small compared to all others, and when it rivals the gap energy¹⁶, the thermal energy, and the energy scale set by the temperature dependence of the chemical potential. The $5/3$ scaling exponent cannot be derived from classical transport equations, and may reflect a nonlinear coupling between different energy scales, common to hydrodynamic systems¹⁷. Whatever the underlying physical mechanism, the observed universal behaviour over decades in field and temperature permits predictive power for $\text{Ag}_{2+\delta}\text{Se}$ sensor response, with every expectation of magnetic field sensitivity well beyond 10^6 G . □

Methods

High-purity Ag_2Se was ground and loaded into outgassed fused silica ampoules inside a helium glove-box, and appropriate amounts of silver were added to reach the desired compositions. The samples were sealed under vacuum, heated in a rocking furnace above its melting point for 24 h, and left to cool in a horizontal position. Regularly shaped sensors of millimetre dimensions were cut on a diamond saw. Electrical leads could be attached easily with either silver epoxy or ultrasonically soldered InBi contacts. Rapid thermal cycling between liquid helium and room temperature can lead to initial changes of the resistance up to 5%, but sample characteristics stabilize after 5 to 7 quenches with no further changes. The variations appear to be dominated by shifts in the relative positions

and quality of the electrical contacts. Lithographically defining micrometre-sized contact pads should improve reproducibility, and would permit the fabrication of submillimetre-sized sensors. Encapsulation in any thermally matched material (such as epoxy) for protection should not hinder performance.

Received 17 December 2001; accepted 2 April 2002.

- Xu, R. *et al.* Large magnetoresistance in non-magnetic silver chalcogenides. *Nature* **390**, 57–60 (1997).
- Chuprakov, I. S. & Dahmen, K. H. Large positive magnetoresistance in thin films of silver telluride. *Appl. Phys. Lett.* **72**, 2165–2167 (1998).
- Ogorelec, Z., Hamzic, A. & Basletic, M. On the optimization of the large magnetoresistance of Ag_2Se . *Europhys. Lett.* **46**, 56–61 (1999).
- Schnyders, H. S., Saboungi, M.-L. & Rosenbaum, T. F. Magnetoresistance in n- and p-type Ag_2Te : Mechanisms and applications. *Appl. Phys. Lett.* **76**, 1710–1712 (2000).
- Abrikosov, A. Quantum magnetoresistance. *Phys. Rev. B* **58**, 2788–2794 (1998).
- Abrikosov, A. Quantum linear magnetoresistance. *Europhys. Lett.* **49**, 789–793 (2000).
- Boebinger, G. S., Lacerda, A. H., Schneider-Muntau, H. J. & Sullivan, N. The National High Magnetic Field Laboratory's pulsed magnetic field facility in Los Alamos. *Physica B* **294–295**, 512–518 (2001).
- Mackay, K., Bonfim, M., Givord, D. & Fontaine, A. 50 T pulsed magnetic fields in microcoils. *J. Appl. Phys.* **87**, 1996–2002 (2000).
- von Ortenberg, M. *et al.* The Humboldt high magnetic field center at Berlin. *Physica B* **294–295**, 568–573 (2001).
- Drndic, M., Johnson, K. S., Thywissen, J. H., Prentiss, M. & Westervelt, R. M. Micro-electromagnets for atom manipulation. *Appl. Phys. Lett.* **72**, 2906–2908 (1998).
- Kohler, M. Zur magnetischen Widerstandsänderung reiner Metalle. *Ann. Phys.* **32**, 211–218 (1938).
- Pippard, A. P. *Magnetoresistance in Metals* (Cambridge Univ. Press, Cambridge, 1989).
- McKenzie, R. H., Qualls, J. S., Han, S. Y. & Brooks, J. S. Violation of Kohler's rule by the magnetoresistance of a quasi-two-dimensional organic metal. *Phys. Rev. B* **57**, 11854–11857 (1998).
- Harris, J. M. *et al.* Violation of Kohler's rule in the normal state magnetoresistance of $\text{YBa}_2\text{Cu}_3\text{O}_{7-\delta}$ and $\text{La}_{2-x}\text{Sr}_x\text{CuO}_4$. *Phys. Rev. Lett.* **75**, 1391–1394 (1995).
- Herring, C. Effect of random inhomogeneities on electrical and galvanomagnetic measurements. *J. Appl. Phys.* **31**, 1939–1953 (1960).
- Aliev, S. A. & Aliev, F. F. Band parameters and energy structure of $\beta\text{-Ag}_2\text{Se}$. *Izv. Akad. Nauk SSSR Neorg. Mater.* **21**, 1869–1872 (1985).
- Tritton, D. J. *Physical Fluid Dynamics* (Van Nostrand Reinhold, New York, 1977).

Acknowledgements

We thank H. Hwang, L. P. Kadanoff and H. S. Schnyders for discussions, and the late R. Xu for technical assistance. The work at the University of Chicago and at Argonne National Laboratory was supported by DOE Basic Energy Sciences.

Competing interests statement

The authors declare that they have no competing financial interests.

Correspondence and requests for materials should be addressed to T.F.R. (e-mail: t-rosenbaum@uchicago.edu).

Rapidly recovering hydrogel scaffolds from self-assembling diblock copolypeptide amphiphiles

Andrew P. Nowak*†, Victor Breedveld‡‡, Lisa Pakstis§, Bulent Ozbas§, David J. Pine†‡, Darrin Pochan§ & Timothy J. Deming*†

* Departments of Materials and Chemistry; † Materials Research Laboratory; ‡ Department of Chemical Engineering, University of California, Santa Barbara, California 93106, USA § Department of Materials Science and Engineering and Delaware Biotechnology Institute, University of Delaware, Newark, Delaware 19716, USA

Protein-based hydrogels are used for many applications, ranging from food and cosmetic thickeners to support matrices for drug delivery and tissue replacement^{1–3}. These materials are usually prepared using proteins extracted from natural sources, which can give rise to inconsistent properties unsuitable for medical applications⁴. Recent developments have utilized recombinant DNA methods to prepare artificial protein hydrogels with specific association mechanisms and responsiveness to various stimuli^{5,6}. Here we synthesize diblock copolypeptide amphiphiles containing charged and hydrophobic segments. Dilute solutions of these

copolypeptides would be expected to form micelles; instead, they form hydrogels that retain their mechanical strength up to temperatures of about 90 °C and recover rapidly after stress. The use of synthetic materials permits adjustment of copolymer chain length and composition, which we varied to study their effect on hydrogel formation and properties. We find that gelation depends not only on the amphiphilic nature of the polypeptides, but also on chain conformations— α -helix, β -strand or random coil. Indeed, shape-specific supramolecular assembly is integral to the gelation process, and provides a new class of peptide-based hydrogels with potential for applications in biotechnology.

Diblock copolypeptide amphiphiles were synthesized (Table 1) using transition metal-mediated α -amino-acid N-carboxyanhydride polymerizations, which allow control over polypeptide chain length and composition (see Methods)^{7,8}. The poly(L-lysine-HBr) and poly(L-glutamate sodium salt) domains are highly charged polyelectrolytes at neutral pH and dissolve readily in water⁹. The hydrophobic domains, when sufficiently large, can adopt regular conformations that aggregate and are insoluble in water, namely, rod-like α -helices for poly(L-leucine) and crystalline β -sheets for poly(L-valine)⁹. Many of these diblock amphiphiles were found to form rigid hydrogels when attempts were made to dissolve small quantities (such as 0.25–2.0 wt%) in water. Copolypeptides of identical compositions, but of statistically random sequences, were found never to form hydrogels at all. Most diblock copolymer amphiphiles with narrow chain length distributions (CLD) form micelles and vesicles in water, resulting in free-flowing suspensions^{10–14}.

Micelles and vesicles do not form interconnected networks, and elastic gel properties only arise when the concentration of particles is sufficiently high to pack them into ordered arrays, typically at least 5–10 wt%, which is an order of magnitude larger than in our polypeptide samples. Block copolymer hydrogel formation at low concentrations has only been observed with triblock architectures, where associating domains on the ends of the copolymers act as interchain crosslinks that result in network formation¹⁵. Similarly, biopolymer gels such as gelatin and carrageenan have several association sites along their long polymer backbones¹⁶. Our copolypeptides displayed quite unusual behaviour in that they were assembling to form network structures from short, narrow CLD diblock amphiphilic chains at low concentrations.

To quantitatively investigate the nature of gel formation in these samples, amphiphiles with different amino acids, hydrophilic to hydrophobic ratios and a range of overall lengths were analysed using rheology¹⁷. The results are summarized in Fig. 1a, where the ratio of storage modulus to loss modulus (G'/G'') was measured for

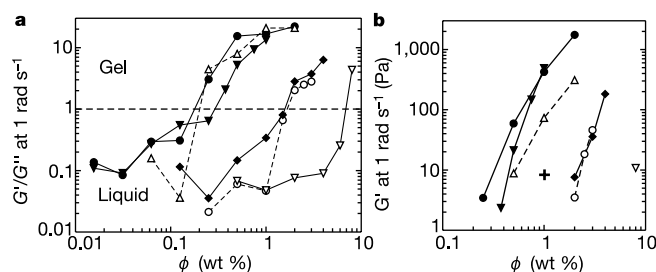


Figure 1 Gelation behaviour of aqueous diblock copolypeptide solutions. **a**, G'/G'' versus concentration ϕ for all samples, at $\omega = 1 \text{ rad s}^{-1}$ ($\phi = [(\text{grams of polymer/grams of sample}) \times 100\%]$). Filled circles, $K_{160}L_{40}$; open circles, $K_{180}L_{20}$; filled down triangles, $K_{160}V_{40}$; open down triangles, $K_{180}V_{20}$; filled diamonds, $K_{160}(\text{rac-L})_{40}$; and open up triangles, $E_{160}L_{40}$; data points are linked to guide the eye. **b**, Gel strength, represented by G' at $\omega = 1 \text{ rad s}^{-1}$, versus concentration for all samples; legend same as in **a** but with crosses indicating $K_{160}L_{40} + 25 \text{ mM NaCl}$.

different polypeptides as a function of concentration. The crossover point where $G' = G''$ provides an accurate measure for the gelation threshold, marking the transition from predominantly viscous to elastic properties. In addition to the ratio G'/G'' , the absolute strengths (G') of the gelled samples are presented in Fig. 1b. For comparison, a 2.0-wt% aqueous gelatin gel was found to possess a strength of $G' = 20 \text{ Pa}$. Because G' for all gels was observed to plateau with increased frequency (see data for $K_{160}L_{40}$ in Fig. 2a), the value at this particular frequency was a good measure of gel strength.

Contrary to most protein gels, which generally dissolve at temperatures greater than 60 °C (ref. 16), these polypeptide gels showed high thermal stability by not visibly thinning up to temperatures as high as 90 °C. Replacement of cationic poly(lysine) segments in $K_{160}L_{40}$ with anionic poly(glutamate) segments ($E_{160}L_{40}$) did not affect hydrogel formation (Fig. 1a). Addition of salt (for example 25 mM NaCl) was found to weaken the gels (Fig. 1b), presumably through screening of polyelectrolyte charges; thus showing that the highly charged segments contribute to gel formation. Accordingly, a similar copolypeptide ($K_{160}^P L_{40}$; where K^P is $\epsilon\text{-CH}_3\text{O}(\text{CH}_2\text{CH}_2\text{O})_2\text{CH}_2\text{C}(\text{O})\text{-L-lysine}$) containing non-charged hydrophilic residues in place of lysine¹⁸, was found not to form aqueous gels at concentrations up to 10 wt%.

The rheology data also revealed trends relating gelation to molecular parameters. The amphiphile $K_{180}L_{20}$ formed gels at concentrations above 2.0 wt%, yet $K_{180}V_{20}$ only formed gels at concentrations above 8.0 wt%. Because L-leucine and L-valine are similarly hydrophobic, the differences in gelation ability might be

Table 1 Abbreviations for diblock copolypeptide amphiphiles

Sample	R ¹	R ²	Proposed conformation
K_xL_y	$-(\text{CH}_2)_4\text{NH}_3^+ \text{Br}^-$	$-\text{CH}_2\text{CH}(\text{CH}_3)_2$	
K_xV_y	$-(\text{CH}_2)_4\text{NH}_3^+ \text{Br}^-$	$-\text{CH}(\text{CH}_3)_2$	
$K_x(\text{rac-L})_y$	$-(\text{CH}_2)_4\text{NH}_3^+ \text{Br}^-$	$-\text{CH}_2\text{CH}(\text{CH}_3)_2$	
E_xL_y	$-\text{CH}_2\text{CH}_2\text{COO}^- \text{Na}^+$	$-\text{CH}_2\text{CH}(\text{CH}_3)_2$	

R¹ and R² refer to amino-acid side-chains (Fig. 3a). K, lysine; L, leucine; V, valine; E, glutamic acid. x, y are number of residues in polymer segments.

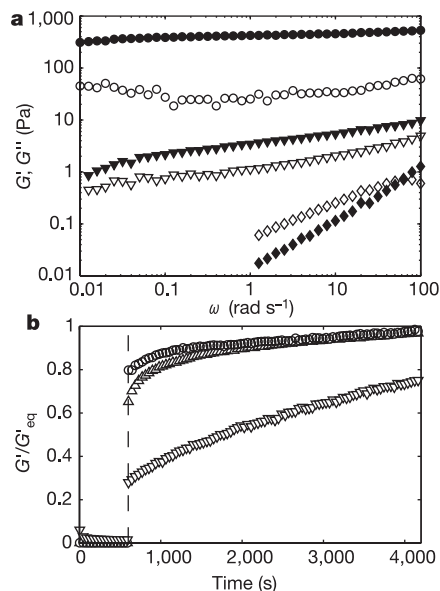


Figure 2 Rheology of diblock copolypeptide solutions. **a**, G' (ω) (filled symbols) and G'' (ω) (open symbols) of $K_{160}L_{40}$ at different concentrations: Diamonds, 0.125 wt%; down triangles, 0.25 wt%; and circles, 1 wt%. The crossover of G' and G'' in the 0.125-wt% sample is an artefact attributable to limitations of the measuring geometry (gap loading limit) and is thus not a relaxation time. **b**, Recovery of gel strength G' for: open up triangle,

1.0-wt% $K_{160}L_{40}$; open circle, 0.75-wt% $K_{160}V_{40}$; open down triangle, 2.0-wt% gelatin. Large-amplitude oscillatory breakdown (1,000% at 6 rad s^{-1} for 600 s) was followed by linear recovery measurements (0.3–1.0% at 6 rad s^{-1}). G' is normalized to the equilibrium gel strength G'_{eq} at 6 rad s^{-1} (see, for example, **a**) to facilitate sample comparison.

due to the conformational differences of the hydrophobic segments. Upon increasing the hydrophobe content to 20 mol%, both $K_{160}L_{40}$ and $K_{160}V_{40}$ were able to form hydrogels at concentrations above 0.4 wt%, with $K_{160}L_{40}$ gelling at a slightly lower concentration than $K_{160}V_{40}$. In these samples, both hydrophobic domains were found

to adopt their expected ordered conformations (Fig. 3c, d), suggesting that both the α -helical and β -strand structures promote gelation. The marked loss of β -structure in going from $K_{160}V_{40}$ to $K_{180}V_{20}$, compared to the negligible change in α -helix content in going from $K_{160}L_{40}$ to $K_{180}L_{20}$ (Fig. 3c, d), correlated well with their

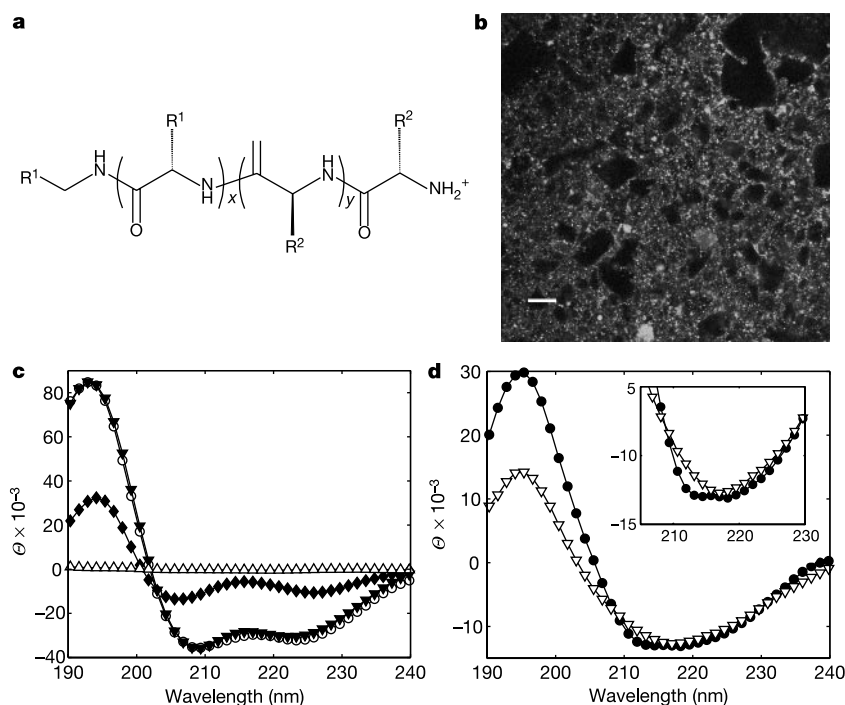


Figure 3 Molecular conformation of diblock copolypeptides. **a**, Generalized molecular structure for all samples (see Table 1 for side groups). **b**, Confocal image of 1-wt% $K_{160}L_{40}$ gel; scale bar, 20 μm . **c**, Circular dichroism spectra (molar ellipticity, Θ , in degrees $\text{cm}^2 \text{dmol}^{-1}$) of leucine-containing samples: Filled down triangle, (rac- K) $_{160}L_{40}$;

open circle, (rac- K) $_{180}L_{20}$; diamond, (rac- K) $_{90}L_{10}$; and open up triangle, (rac- K) $_{160}$ (rac- L) $_{40}$. **d**, Circular dichroism spectra of valine-containing samples: Filled circle, (rac- K) $_{180}V_{20}$; and open up triangle, (rac- K) $_{160}V_{40}$. Inset shows expanded detail of spectra.

respective decreases in gel-forming ability. Similarly, a copolypeptide of lower molecular weight, $K_{90}L_{10}$, where the helical conformation of the leucine domain was now greatly disordered because of its short length (Fig. 3c), also showed no tendency to form a gel up to concentrations as high as 8.0 wt%. These results suggest that stable chain conformations are essential in the formation and strength of these hydrogels.

To examine chain conformation explicitly we used rheological analysis of a $K_{160}(\text{rac-L})_{40}$ copolypeptide where the poly(leucine) segment contained a statistical sequence of equal proportions of L- and D-leucine residues. This hydrophobic segment, although compositionally identical to poly(L-leucine), cannot adopt the α -helical conformation because of unfavourable side-chain interactions (Fig. 3c)⁹. The substitution of this conformationally random segment resulted in a significant increase of gelation threshold (0.25 to 2.0 wt%; Fig. 1a). Therefore, it appeared that gelation is tied to the conformations of the hydrophobic domains, where α -helical segments are slightly better gelators than β -strands, which are better than random coils.

This correlation suggests that the self-assembly process is conformation-specific at the molecular level, similar to protein assembly. The specificity of these interactions was further illustrated by mixing equal amounts of $K_{160}L_{40}$ and $K_{160}(\text{rac-L})_{40}$ such that the final concentrations of each amphiphile were 0.25 wt%. If these amphiphiles could cooperate, the total amount of copolymer (0.50 wt%) should have resulted in a rigid hydrogel. However, the G' measured for this sample was lower than that of a 0.25-wt% solution of $K_{160}L_{40}$ alone. This result indicated that $K_{160}(\text{rac-L})_{40}$ was not only unable to cooperate in hydrogel formation, but also disrupted packing of the helical chains in $K_{160}L_{40}$. Similarly, chain length was found to be important in the specificity of assembly because an analogous mixture of $K_{160}L_{40}$ and $K_{180}L_{20}$ —in effect, a simulated increase in hydrophobic CLD—was found to lower G' relative to the individual components.

Although the rheological studies were sensitive to changes in macroscopic structure, they did not reveal details about the underlying gel microstructure. To study their morphology, the gels were visualized using cryogenic transmission electron microscopy (CTEM) and laser scanning confocal microscopy (LSCM), where a small amount of fluorescent hydrophobic dye was used to label the self-assembled hydrophobic matrix. In Fig. 3b and in the Supplementary Information, images are shown of a typical gel ($K_{160}L_{40}$) at concentrations matching those of rheology measurements in Fig. 2a. As concentration was increased from the free-flowing 0.125-wt% solution to the 1.00-wt% hydrogel, the images showed a progression from loosely connected fragments of dyed polypeptide-containing domains to a dense microscopic network interspersed with polymer-free liquid regions. Thus, as concentration was increased, hydrogel formation appeared to coincide with intergrowth of microscopically phase-separated domains of 1–25 μm in size. This heterogeneity suggests that the block copolypeptides preferentially segregate into gel matrix domains that exclude some fraction of the available water. CTEM visualization of the vitrified gel domains (Supplementary Information) revealed a complex membrane assembly responsible for network formation at the nanoscale. Similar morphologies were observed for all other hydrogel-forming polypeptide amphiphiles.

The porous nature of the copolypeptide gels was verified using microrheological experiments. This technique relies on the measurement of thermally induced brownian motion of micro-metre-size tracer particles dispersed in the sample^{19,20}. In a 0.25-wt% $K_{160}L_{40}$ gel it was observed that tracer particles of 0.5 μm diameter diffused freely as if suspended in a liquid environment (that is, their mean-square displacement, MSD, increased linearly with time), whereas 1.0- μm particles showed restricted motion (MSD reached a plateau over time) as they began to experience some confinement. This shift in behaviour was consistent with both

the LSCM and earlier rheological data (Fig. 2a) in that the larger 1.0- μm tracers should experience some restraint as they are near the lower size limit of the voids. Microrheology confirmed the existence of microscopic heterogeneity in these hydrogels, which was found to persist after prolonged standing, heating, centrifugation, and bulk shear of the samples.

This morphology is unusual in that most hydrogels are heterogeneous at short length scales (<100 nm), but homogenous at the microscopic level^{1–4}. In the copolypeptides, the hydrophobic associations must be sufficiently strong to stop the swelling driven by electrostatic repulsion of the polyelectrolyte segments. The strength of these associations probably originates from the ordered packing of the α -helical and β -strand segments. The resulting porous structure represents a balance of these competing attractive and repulsive forces, and may prove advantageous in developing these materials via suitable engineering for biotechnology applications where diffusion of large molecules (for example, proteins, DNA) through the voids²¹, entrapment and proliferation of cells for tissue regeneration²², or the biomimetic confined nucleation of inorganic phases^{23,24} are desired.

The dynamics of the gelation process were also investigated. In the rheometer, the polymer gels were subjected to large amplitude oscillations to break down the gel structure. The recovery of the gels was then probed by measuring G' and G'' in the linear, small deformation regime as a function of time. Within the short time that had elapsed in between switching amplitudes (about 10 s), the hydrogels had recovered 80–90 % of their strength, followed by a slower reorganization process where the full initial value of G' was restored (Fig. 2b). This rapid recovery can be attributed to the physical nature of gelation and the relatively low relative molecular mass of the copolypeptides, which enables the molecules to reorganize quickly. Gelatin gels, because of the low mobility of large macromolecules, recover only slowly after being broken down by shear. The low gelation concentrations (~1.0 wt%) for these polypeptides can also be contrasted with surfactant-based hydrogels that require considerable amounts of low relative molecular mass lipid (20–50 wt%) to achieve gelation²⁵. The exceedingly low mass fraction of material in the polypeptide hydrogels, combined with their recovery properties and microporous structure, allows them to fill an advantageous and unique niche in between conventional polymer and surfactant hydrogels. Their peptide backbone also imparts to these materials advantageous features of proteins (such as degradability and functionality), which makes them attractive for biomedical applications. □

Methods

Synthesis

All block copolypeptides were synthesized using $\text{Co}(\text{PMe}_2)_4$ initiator²⁶, and were purified and then characterized using size exclusion chromatography, ¹H and ¹³C nuclear magnetic resonance (NMR), and infrared spectroscopy according to literature procedures². Isolated yields of the final copolymers ranged between 75% and 90%. Amino-acid compositions of the copolymers were found to be within 3% of predicted values. Chain lengths of the copolymers were found to be within 8% of predicted lengths with CLD (weight average length/number average length) ranging between 1.1 and 1.3 (Supplementary Information).

Circular dichroism

Copolypeptides, 0.5 mg ml⁻¹ in deionized water, were analysed in a 0.5-mm path length quartz cell on an Olis RSM 1000 Spectrometer. Samples analogous to $K_{160}L_{40}$, $K_{160}V_{40}$, $K_{180}L_{20}$, $K_{90}L_{10}$, $K_{160}(\text{rac-L})_{40}$, and $K_{180}V_{20}$ were prepared using racemic D/L-lysine to eliminate contributions of the polylysine domain from the CD spectra²⁷. The approximate conformations of the hydrophobic domains were determined using the method of Fasman²⁸. $K_{160}L_{40}$ and $K_{180}L_{20}$: 90% α -helix, 10% random coil. $K_{90}L_{10}$: 50% α -helix, 50% random coil. $K_{160}(\text{rac-L})_{40}$: no optical activity. $K_{160}V_{40}$: 80% β -sheet, 20% random coil. $K_{180}V_{20}$: 40% β -sheet, 40% α -helix, 20% random coil (note the double minimum for $K_{180}V_{20}$ in Fig. 3d indicating the presence of partial α -helical structure).

Rheology

Rheological measurements were performed on a Rheometrics ARES controlled strain rheometer in cone-plate geometry with 50 mm diameter and 2° cone angle. For each sample, small-deformation linearity was checked before performing oscillatory

measurements. All hydrogels were prepared by dissolving freeze-dried polypeptide powder in deionized water. To speed up dissolution, vortex mixing was also applied for a few minutes to the samples, although identical samples could be prepared without agitation by letting them stand overnight. Gelatin samples were prepared by dissolving the protein in warm water (60 °C).

Microrheological measurements were performed by dispersing a small amount of monodisperse polystyrene spheres (with amidine surface groups) into copolymer solutions of $K_{160}L_{40}$. The brownian motion of the tracer particles was captured by digital video microscopy in a conventional microscope (Nikon) with 100 × oil-immersion objective. Image analysis was performed with IDL software. Particle trajectories were extracted and analysed using algorithms developed and kindly provided by the Weitz group (Harvard University)¹⁹.

Microscopy

For LSCM, lipophilic fluorescent dye (DiOC₁₈, Molecular Probes) was dissolved (about 0.001 wt%) in THF. Several drops of this dye solution were added to deionized water that was used to prepare the hydrogels, which were allowed to stand for over 12 h before imaging. Imaging was performed with a Zeiss 510 microscope equipped with an ArKr laser (30 mW) using 488 nm as the excitation line for the dye. For CTEM, a 1.0-wt% sample of $K_{160}L_{40}$ was spread into a thin film on glass, into which a carbon-coated TEM grid was pressed, thus transferring a thin film of sample. The hydrated gel was then vitrified on the grid in liquid ethane with a Leica cryoplunging system. The *in situ*, vitrified gel membrane scaffolding was subsequently directly imaged without staining at 200 kV in bright-field mode using a Gatan 626 cryotransfer stage in a JEOL 2000FX microscope.

Received 22 October 2001; accepted 5 April 2002.

- Okano, T. (ed.) *Biorelated Polymers and Gels* (Academic, San Diego, 1998).
- Dagani, R. Intelligent gels. *Chem. Eng. News* **75**, 23, 26–37 (1997).
- Peppas, N. A., Huang, Y., Torres-Lugo, M., Ward, J. H. & Zhang, J. Physicochemical foundations and structural design of hydrogels in medicine and biology. *Annu. Rev. Biomed. Eng.* **2**, 9–29 (2000).
- Ward, A. G. & Courts, A. (eds) *The Science and Technology of Gelatin* (Academic, London, 1977).
- Petka, W. A., Harden, J. L., McGrath, K. P., Wirtz, D. & Tirrell, D. A. Reversible hydrogels from self-assembling artificial proteins. *Science* **281**, 389–392 (1998).
- Wang, C., Stewart, R. J. & Kopeček, J. Hybrid hydrogels assembled from synthetic polymers and coiled-coil protein domains. *Nature* **397**, 417–420 (1999).
- Deming, T. J. Facile synthesis of block copolypeptides of defined architecture. *Nature* **390**, 386–389 (1997).
- Deming, T. J. Cobalt and iron initiators for the controlled polymerization of alpha-amino acid-N-carboxyanhydrides. *Macromolecules* **32**(13), 4500–4502 (1999).
- Katchalski, E. & Sela, M. Synthesis and chemical properties of poly-α-amino acids. *Adv. Protein Chem.* **13**, 243–492 (1958).
- Buitenhuis, J. & Forster, S. Block copolymer micelles: viscoelasticity and interaction potential of soft spheres. *J. Chem. Phys.* **107**(1), 262–272 (1997).
- Guenoun, P. *et al.* Polyelectrolyte micelles: self-diffusion and electron microscopy studies. *Langmuir* **16**(10), 4436–4440 (2000).
- Hamley, I. W. *et al.* From hard to soft spheres: the effect of copolymer composition on the structure of micellar cubic phases formed by diblock copolymers in aqueous solution. *Langmuir* **16**(6), 2508–2514 (2000).
- Won, Y.-Y., Davis, H. T. & Bates, F. S. Giant wormlike rubber micelles. *Science* **283**, 960–963 (1999).
- Moffitt, M., Khougaz, K. & Eisenberg, A. Micellization of ionic block copolymers. *Acc. Chem. Res.* **29**, 95–102 (1996).
- Tsitilianis, C., Iliopoulos, I. & Ducouret, G. An associative polyelectrolyte end-capped with short polystyrene chains. Synthesis and rheological behaviour. *Macromolecules* **33**(8), 2936–2943 (2000).
- Clark, A. C. & Ross-Murphy, S. B. Structural and mechanical properties of biopolymer gels. *Adv. Polym. Sci.* **83**, 57–192 (1987).
- Kavanagh, G. M. & Ross-Murphy, S. B. Rheological characterisation of polymer gels. *Prog. Polym. Sci.* **23**(3), 533–562 (1998).
- Yu, M., Nowak, A. P., Pochan, D. P. & Deming, T. J. Methylated mono- and diethyleneglycol functionalized polylysines: nonionic, helical, water soluble polypeptides. *J. Am. Chem. Soc.* **121**, 12210–12211 (1999).
- Crocker, J. C. *et al.* Two-point microrheology of inhomogeneous soft materials. *Phys. Rev. Lett.* **85**(4), 888–891 (2000).
- Mason, T. G. & Weitz, D. A. Optical measurements of frequency-dependent linear viscoelastic moduli of complex fluids. *Phys. Rev. Lett.* **74**(7), 1250–1253 (1995).
- Liu, L., Li, P. & Asher, S. A. Entropic trapping of macromolecules by mesoscopic periodic voids in a polymer hydrogel. *Nature* **397**, 141–144 (1999).
- Lee, K. Y. & Mooney, D. J. Hydrogels for tissue engineering. *Chem. Rev.* **101**, 1869–1880 (2001).
- Falini, G., Fermani, S., Gazzano, M. & Ripamonti, A. Polymorphism and architectural crystal assembly of calcium carbonate in biologically inspired polymeric matrices. *J. Chem. Soc. Dalton* **21**, 3983–3987 (2000).
- Cha, J. N., Stucky, G. D., Morse, D. E. & Deming, T. J. Biomimetic synthesis of ordered silica structures mediated by block copolypeptides. *Nature* **403**, 289–292 (2000).
- Hoffmann, H. & Ulbricht, W. Surfactant gels. *Curr. Opin. Colloid Interf. Sci.* **1**, 726–739 (1996).
- Klein, H. F. & Karsch, H. H. Methylcobalt compounds with non-chelating ligands. 1. Methyltetraakis(trimethylphosphine) cobalt and its derivatives. *Chem. Ber.* **108**(3), 944–955 (1975).
- Kubota, S. & Fasman, G. Conformation and optical properties of poly(L-valine) in aqueous solution. “A single extended β chain.” *J. Am. Chem. Soc.* **96**, 4684–4686 (1974).
- Adler, A. J., Greenfield, N. J. & Fasman, G. D. Circular dichroism and optical rotary dispersion of proteins and polypeptides. *Methods Enzymol.* **27**, 675–735 (1973).

Supplementary Information accompanies the paper on Nature's website (<http://www.nature.com>).

Acknowledgements

This work was supported by grants from the National Science Foundation (Chemical and Transport Systems, and MRSEC Program). V.B. thanks the Netherlands Organization for Scientific Research (NWO) for a Talent-grant. We thank J. Hu for assistance with NMR experiments.

Competing interests statement

The authors declare that they have no competing financial interests.

Correspondence and requests for materials should be addressed to T.J.D. (e-mail: tdeming@mrl.ucsb.edu).

Low slip rates and long-term preservation of geomorphic features in Central Asia

Ralf Hetzel*†‡, Samuel Niedermann*, Mingxin Tao‡, Peter W. Kubik§, Susan Ivy-Ochs||, Bo Gao‡ & Manfred R. Strecker†

* *GeoForschungsZentrum Potsdam, Telegrafenberg, D-14473 Potsdam, Germany*

† *Institut für Geowissenschaften, Universität Potsdam, D-14415 Potsdam, Germany*

‡ *The State Key Laboratory of Gas-geochemistry, Lanzhou Institute of Geology, Chinese Academy of Science, 324 Donggang West Avenue, Lanzhou 730000, China*
§ *Paul Scherrer Institut, c/o the Institute of Particle Physics; and the || Institute of Particle Physics, ETH Hönggerberg, CH-8093 Zurich, Switzerland*

In order to understand the dynamics of the India–Asia collision zone, it is important to know the strain distribution in Central Asia, whose determination relies on the slip rates for active faults^{1–5}. Many previous slip-rate estimates of faults in Central Asia were based on the assumption that offset landforms are younger than the Last Glacial Maximum (~20 kyr ago)^{6–11}. In contrast, here we present surface exposure ages of 40 to 170 kyr, obtained using cosmogenic nuclide dating, for a series of terraces near a thrust at the northern margin of the Tibetan Plateau. Combined with the tectonic offset, the ages imply a long-term slip rate of only about 0.35 mm yr⁻¹ for the active thrust, an order of magnitude lower than rates obtained from the assumption that the terraces formed after the Last Glacial Maximum. Our data demonstrate that the preservation potential of geomorphic features in Central Asia is higher than commonly assumed.

The ongoing collision between India and Eurasia has caused widespread Cenozoic deformation resulting in uplift of the Himalayas, the Tibetan Plateau and other mountain ranges in Central Asia¹² (Fig. 1a). The present rate of convergence between India and Eurasia is of the order of 40–50 mm yr⁻¹ (see ref. 13), with only 18 ± 2 mm yr⁻¹ being accommodated by Himalayan thrusts¹⁴. The remaining 20–30 mm yr⁻¹ of convergence are distributed on faults in actively growing mountain ranges farther north. Ideally, slip rates of active faults are determined by dividing measured tectonic offsets by well constrained ages for the faulted geomorphic markers, as, for example, has been achieved along the Kunlun fault¹⁵. However, many slip rates in Central Asia have been based on offset geomorphic features which were assumed to have formed after the Last Glacial Maximum (~20 kyr ago)^{6–11}. In Central Asia the maximum advance of glaciers apparently occurred well before 20 kyr ago, so tectonically offset landforms may in fact be much older¹⁶. This seems to be the case for the central Altyn Tagh fault at the northern boundary of the Tibetan Plateau, where inferred ages of faulted landforms result in a high slip rate of 20–30 mm yr⁻¹ (ref. 6), while